In: ISABE 2017: 23rd International Symposium on Air Breathing Engines: Economy, Efficiency and Environment, 3-8 September 2017, Manchester, UK. Paper number: ISABE-2017-21476

Modelling and performance analysis of vaneless counter rotating turbine in gas turbine engines

Linyuan Jia, Yuchun Chen, Yuan Gao
jlynpu@mail.nwpu.edu.cn
Northwestern Polytechnical University
School of Power and Energy
Xi'an Shaanxi
China

Junjie Zhao
Cranfield University
School of Aerospace, Transport and Manufacturing (SATM)
Cranfield Bedford
U.K

ABSTRACT

The objective of this article is to develop a method for 1+1/2 type vaneless counter rotating turbine (VCRT) modelling in gas turbine engines and to analyse the influence of the VCRT on a turbofan engine. By studying the off-design features of the VCRT, a new method to describe the VCRT characteristic map was established. The new turbine maps were integrated into the gas turbine performance simulation model based on component maps. The throttle performance of a low bypass counter rotating turbofan engine was simulated and the results were validated with engine test data. The validation results show that the new method improves the accuracy of the VCRT engine performance simulation. The influence of the VCRT on the engine steady state performance was illuminated by comparing the performance of a VCRT engine with that of a conventional engine. Under low engine load conditions, the insufficient work capacity of the VCRT low pressure turbine was detected due to the decrease of both its efficiency and pressure ratio. Consequently, the VCRT engine's turbine inlet temperature, fan rotating speed, mass flow rate and engine thrust decreased while its specific fuel consumption increased compared to that of a conventional engine.

Keywords: Vaneless counter rotating turbine, gas turbine engine performance simulation, turbine characteristic maps, velocity triangle

Proceedings ISBN: 978-1-5108-7279-0. Please refer to any applicable publisher terms of use.

NOMENCLATURE

VCRT	Vaneless counter rotating turbine
NPSS	Numerical Propulsion System Simulation
HP	High pressure
LP	Low pressure

Symbols

C	Absolute velocity [m/s]	P	Total pressure [Pa]
Cp	Specific heat capacity [J/(kg·K)]	Ps	Static pressure [Pa]
F_N	Nominal engine thrust [N]	T	Total temperature [K]
f	Function [-]	U	Circumferential velocity [m/s]
k	Ratio of specific heat capacity [-]	W	Relative velocity [m/s]
L	Work of turbo machinery [W]	Wfb	Combustor fuel flow rate [kg/s]
l	Specific work of turbo machinery [W/kg]	π	Pressure ratio [-]
Ma	Mach number [-]	η	Efficiency [-]
m	Mass flow rate [kg/s]	β	Beta value for compressor map [-]
N	Rotating speed of spool [1/min]	ERR	Error equations

Subscripts

a	Air	h	High pressure part
c	Compressor	in	inlet
cor	Corrected value	l	Low pressure part
core	Core part of the fan	r	Required value
duct	Duct part of the fan	t	Turbine
f	Fan	u	Circumferential component
g	gas	des	Design condition

1.0 INTRODUCTION

The thrust-to-weight ratio, which is a major parameter to judge the advancement of a supersonic propulsion system, is becoming higher and higher as the demand for airplane performance grows. Encouraged by this trend, many advanced technologies have been investigated, and the VCRT technology is regarded as one of the most promising.[1, 2]

The VCRT referred to in this article is the 1+1/2 type. In this kind of turbine, the high pressure (HP) turbine stage consists of one row of stator vanes and one row of rotor blades, while the low pressure (LP) turbine stage has only one row of rotor blades. The rotational direction of the HP rotor is contrary to that of the LP rotor, thus making the HP turbine blades able to provide the prewhirl for LP turbine blades. Consequently, LP guide vanes are eliminated. On one hand, the elimination of LP guide vanes contributes to shorter and lighter engine structures, thus increasing the engine thrust-to-weight ratio. On the other hand, counter rotating of the two rotors decreases the gyroscopic couple of the airplane during flight maneuvers, which ensures better airplane maneuverability.[3, 4]

An essential step in the research of the VCRT technology is to simulate its performance in a gas turbine engine. Gas turbine engine performance simulation models have been built up to have different levels of fidelity and complexity. The famous Numerical Propulsion System Simulation (NPSS)[5, 6] and the de-coupled gas turbine engine simulation model developed by Pachidis et al[7, 8]. are able to simulate the engine performance and provide three-dimensional component inner flow fields. However the most practical and widely used engine performance simulation model is the component maps based performance simulation model. It was first published by the NASA Lewis Research Centre in 1975.[9] Its component maps based structure and off-design points matching technique have laid the foundation for many gas turbine engine performance simulation software such as the well-known Gasturb and the Gasturbine Simulation Program (GSP).[10, 11] Since the component maps based model provides enough detail for engine performance design and analysis, it was chosen to simulate the performance of a VCRT turbofan engine.

The key of a high fidelity engine performance simulation, which uses the component maps based model, is appropriate component characteristic maps that represent the performance of each component. The more accurate the maps are, the closer the results reach the real performance of the engine. Therefore, accurate VCRT characteristic maps are essential to simulate the performance of a VCRT gas turbine engine.

A literature review was done to find descriptions of VCRT characteristic maps. Systematic research was carried out regarding a VCRT's aerodynamic design,[12, 13] hot streak effect,[14, 15] off-design condition flow control,[16] and cooling of turbine assemblies[17] at the Institute of Engineering Thermophysics (IET) at the Chinese Academy of Sciences (CAS). Experimental work was also done by other researchers to demonstrate the VCRT's capability to increase the gas turbine engine's thrust-to-weight ratio.[1, 18, 19] The effects of speed ratio on the performance and flow field of a counter rotating turbine was investigated by means of the CFD simulation.[20]

However, the studies mentioned above were either focused on the design and optimization of turbine elements or the analysis of flow field details. The description and application of VCRT characteristic maps in an engine performance simulation model are not yet discussed.

In this study, a new method was brought forward to describe VCRT characteristic maps by considering the influence of the HP turbine rotor on the LP turbine performance. Then the performance of a counter rotating turbofan engine was simulated and the method was validated using engine test data. With this method, the influence of a VCRT on the steady state performance of a turbofan engine was analysed.

2.0 MODELING OF THE VCRT

Appropriate characteristic maps of the VCRT are essential to the performance modelling of a VCRT engine. In this section, the off-design features of the VCRT are analysed initially in terms of the velocity triangle. Based on the analysis, the characteristic maps of the HP turbine and the LP turbine in a VCRT are described separately. Then the newly generated VCRT maps are integrated into the simulation model for a low bypass turbofan engine.

2.1 Off-design features of the VCRT.

As is shown in Figure 1, in a VCRT, the HP rotor provides the preswirl for the LP rotor directly as a consequence of the elimination of LP guide vanes. The HP turbine operating condition determines the velocity triangle and further influences the performance of the LP turbine. The velocity triangle method, introduced by Ji L,[3] is used here to analyse the off-design features of the VCRT. The analysis can be performed from two aspects. One is varying the HP stage back pressure, the other is varying the HP rotor rotational speed. Note that this section does not offer precise quantitative analyses. Instead, it is based on theoretical analysis which illuminates how the HP turbine influences the LP turbine.

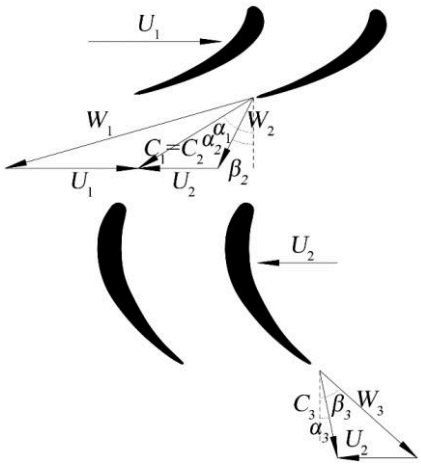

Figure 1. Velocity triangles of vaneless counter rotating turbine

In Figure 1, U_1 and U_2 stand for the rotational speeds of the HP rotor and the LP rotor respectively. W_1 denotes the relative outflow velocity of the HP rotor, and W_2 the relative inflow velocity of the LP rotor. C_1 equals C_2 and stands for the absolute outflow velocity of the HP rotor, or the absolute inflow velocity of the LP rotor, and C_3 the absolute outflow velocity of the LP rotor. α_1 equals α_2 and denotes the absolute flow angle between the HP and LP rotor, α_3 the LP rotor outflow angle. β_2 and β_3 represent the relative in- and outflow angles of the LP rotor.

2.1.1 Varying back pressure.

In this case, the rotational speed of the HP rotor is kept constant. The magnitude of the relative outflow velocity of a blade row changes with varying back pressure. So the off-design operation of varying back pressure can be presented in terms of how the changed relative outflow velocity of the HP turbine influences the velocity triangle and the performance of the LP turbine. The HP turbine relative outflow velocity increases as a consequence of decreasing HP rotor back pressure, see Figure 2.

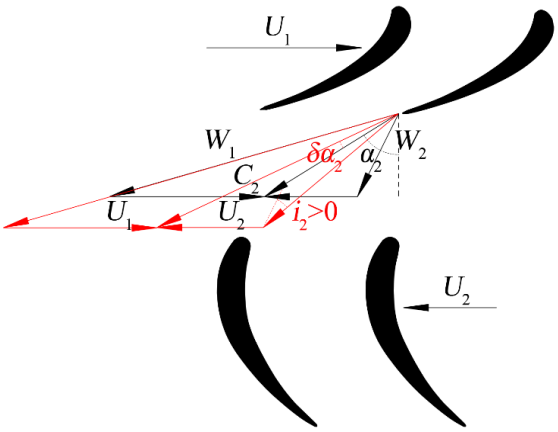

Figure 2 Varying back pressure

The main changes of the velocity triangle and their influences on the LP turbine performance can be drawn as follows.

1. Assume that the velocity triangle denoted by black vectors in Figure 2 provides the ideal angle of incidence for the LP rotor. The LP turbine efficiency decreases due to increased angle of incidence of the LP rotor.

2. The mass flow of the LP turbine increases as a consequence of an increase of the meridianal component of the LP rotor inflow velocity, see $C_2 cos\alpha_2$ in Figure 2.

3. The LP turbine pressure ratio is closely related to the LP turbine's specific work. Equation (1) and equation (2) define the turbine specific work in different terms. The former is in terms of the velocity triangle and the latter in terms of thermodynamic parameters.

$$l_t = U_2 (C_3 sin\alpha_3 + C_2 sin\alpha_2) \quad \dots (1)$$

$$l_t = Cp_g T_{in} (1\text{-}1 / \pi_t^{(k-1)/k}) \eta_t \quad \dots (2)$$

From equation (2), the turbine pressure ratio is derived as equation (3). Known from equation (3), the LP turbine pressure ratio increases with an increasing l_t or decreasing η_t.

$$\pi_t = (1 - l_t / Cp_g T_{in} \eta_t)^{-k/(k-1)} \quad \dots (3)$$

C_2 and α_2 in Figure 2 both increase as W_1 increases, thus causing l_t to increase, see equation 1. Additionally, the efficiency decreases as stated in item 1. Known from equation 3, the LP turbine pressure ratio increases as the HP turbine back pressure decreases.

2.1.2 Varying rotational speed.

In this case, the back pressure of the HP stage is kept constant. The velocity triangles of varying rotational speed are shown in Figure 3. Assuming that U_1 increases, shown as dU_1, conclusions can be drawn as follows.

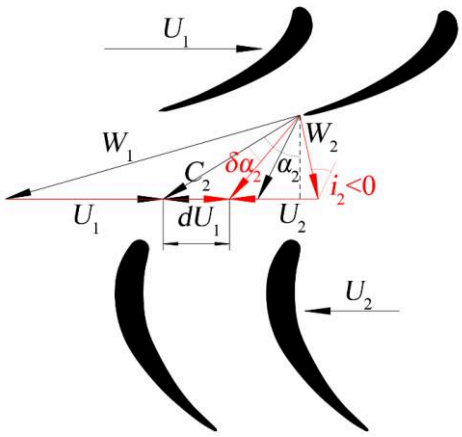

Figure 3. Varying rotational speed

1. Assume that the velocity triangle denoted by black vectors in Figure 3 provides the ideal angle of incidence for the LP rotor. The LP turbine efficiency decreases due to decreased angle of incidence of the LP rotor.

2. The mass flow of the LP turbine remains the same as is the meridianal component of the LP rotor inflow velocity, see $C_2 cos\alpha_2$ in Figure 3.

3. The LP turbine specific work l_t which can be derived as $U \cdot \Delta C_u$ decreases as a consequence of C_2 and α_2 decreasing, which further causes the LP turbine pressure ratio to decrease. Additionally, the efficiency decreases as stated in item 1, which is beneficial for the LP turbine pressure ratio to increase. In this case, the trend of the LP turbine pressure ratio becomes unpredictable.

The velocity triangle analysis above is far from the reality of the VCRT off-design operation due to insufficient consideration of the 3D effect, the flow separation and the viscosity of the gas. Yet it offers a sense of how the HP turbine operating conditions influence the LP turbine performance. In a conventional turbine, these influences are 'filtered' by the stator ahead of the LP rotor which makes the LP turbine independent of the HP turbine's operating condition. While in a VCRT, these influences should not be ignored. The HP turbine back pressure, represented by the pressure ratio, and the HP turbine rotational speed should be introduced into the description of the LP turbine's characteristics.

2.2 Description of VCRT characteristic maps

In this section, the description of the VCRT HP turbine map and the VCRT LP turbine map are discussed and presented separately. The HP turbine maps have the same form as the traditional turbine. For the LP turbine maps, the HP turbine operating parameters, i.e. the pressure ratio and the rotational speed, are introduced into the description to consider their influence on the LP turbine performance.

2.2.1 Description of HP turbine maps.

Since the structure and mechanism of the HP turbine in a VCRT are the same as those of a conventional turbine, the VCRT HP turbine maps should also be the same as conventional turbine maps. In conventional turbine maps, the corrected mass flow, see equation (4), and the efficiency, see equation (5), are described as functions of the corrected rotational speed and the pressure ratio, see Figure 4.

$$m_{h,cor} = f_1(N_{h,cor}, \pi_{t,h}) \quad \ldots (4)$$

$$\eta_{t,h} = f_2(N_{h,cor}, \pi_{t,h}) \quad \ldots (5)$$

For each line in Figure 4, the corrected rotational speed is constant. The corrected mass flow, see Figure 4(a), and the efficiency, see Figure 4(b), change with the pressure ratio. Note that the values in Figure 4 are all relative values compared with design data.

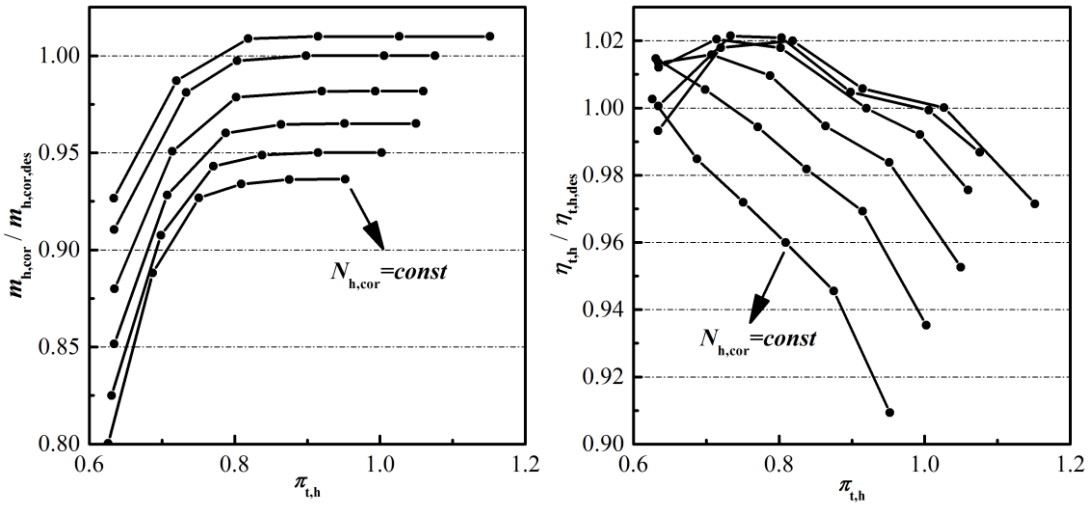

(a) Corrected mass flow vs. pressure ratio (b) Efficiency vs. pressure ratio

Figure 4. HP turbine maps of a VCRT

2.2.2 Description of LP turbine maps.

According to the analysis of the off-design features of the VCRT, the HP turbine back pressure and the rotational speed influence the LP turbine performance. Thus, the HP turbine pressure ratio $\pi_{t,h}$ and corrected rotational speed $N_{h,cor}$ are introduced into the description of VCRT LP turbine characteristic maps. In addition, the LP turbine's own pressure ratio $\pi_{t,l}$ and corrected rotational speed $N_{l,cor}$ are also used. Finally, the LP turbine maps are described as functions of four parameters as shown in equation (6) and (7).

$$m_{l,cor} = f_3(N_{h,cor}, \pi_{t,h}, N_{l,cor}, \pi_{t,l}) \quad \ldots (6)$$

$$\eta_{t,l} = f_4(N_{h,cor}, \pi_{t,h}, N_{l,cor}, \pi_{t,l}) \quad \ldots (7)$$

Among the four variables on the right side of equation (6) and (7), $N_{h,cor}$ and $\pi_{t,h}$ introduce the influence of the HP turbine on the LP turbine, while $N_{l,cor}$ and $\pi_{t,l}$ define the operating condition of the LP turbine. With two additional variables compared to the conventional turbine maps, the VCRT LP turbine maps are more complicated from the aspect of both description and interpolation. However, the LP turbine maps will be the same as conventional turbine maps with fixed values of $N_{h,cor}$ and $\pi_{t,h}$.

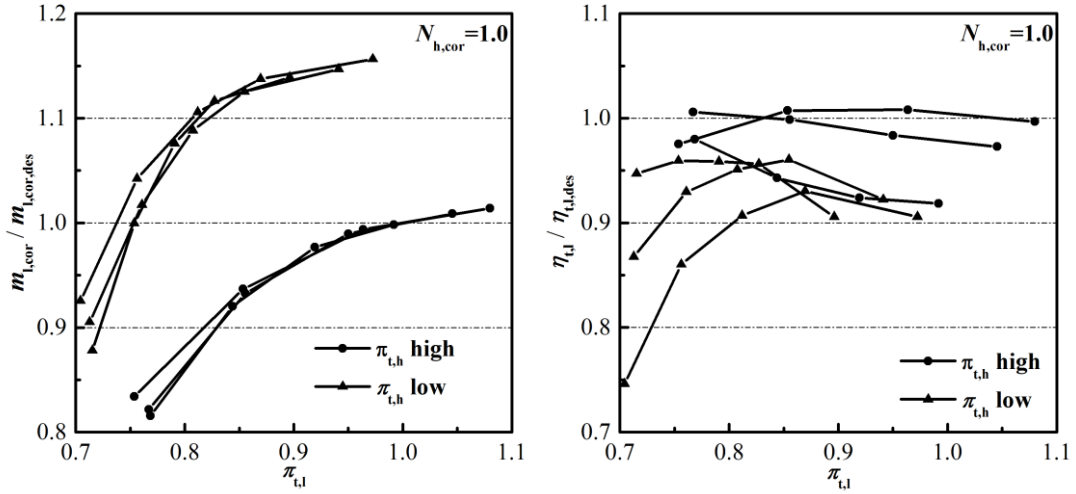

(a) Corrected mass flow vs. pressure ratio (b) Efficiency vs. pressure ratio

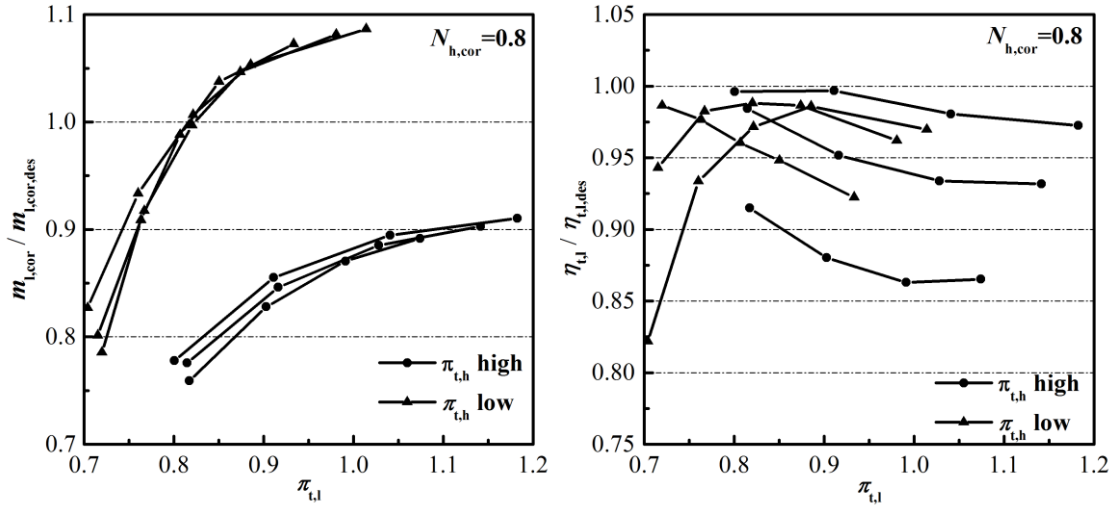

(c) Corrected mass flow vs. pressure ratio (d) Efficiency vs. pressure ratio

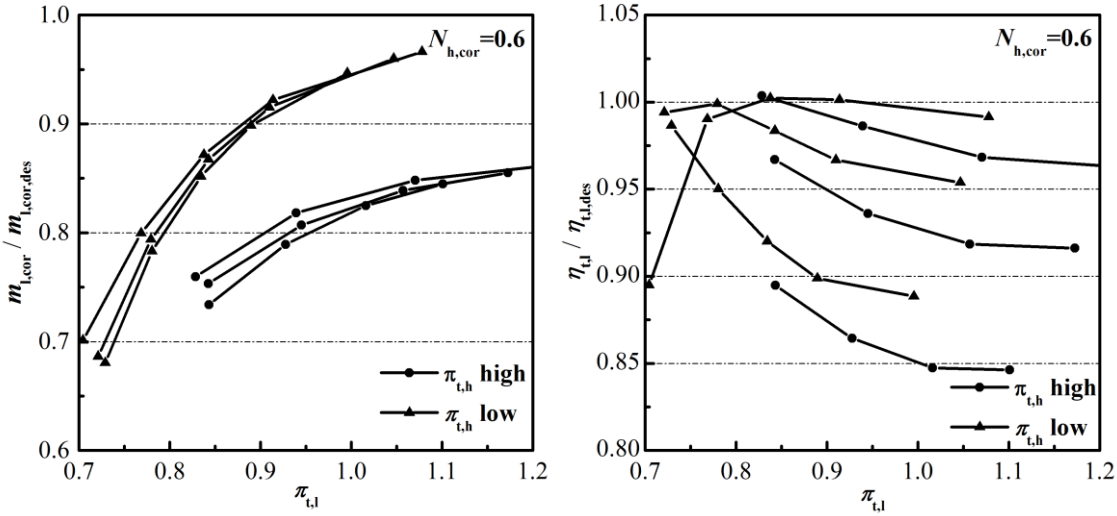

(e) Corrected mass flow vs. pressure ratio (f) Efficiency vs. pressure ratio

Figure 5. Vaneless counter rotating turbine low pressure turbine maps

Figure 5 shows the LP turbine maps of a vaneless counter rotating turbine. All the data provided is the relative value divided by the LP turbine design data. The maps are divided into three groups by means of the variable separation approach according to different values of $N_{h,cor}$. Each group stands for a fixed $N_{h,cor}$ and contains two sets of characteristic data regarding two $\pi_{t,h}$ values. For each line in Figure 5, the LP turbine corrected rotational speed is constant. As stated before, with fixed values of $N_{h,cor}$ and $\pi_{t,h}$, the LP turbine maps are the same as conventional turbine maps. For the purpose of higher fidelity, more $N_{h,cor}$ and $\pi_{t,h}$ groups with a smaller step length are suggested.

Four variables, $N_{h,cor}$, $\pi_{t,h}$, $N_{l,cor}$ and $\pi_{t,l}$, in conjunction with the quaternion interpolation algorithm are required to get the exact values of $m_{l,cor}$ and $\eta_{t,l}$ from the LP turbine maps presented above. The discussion of the quaternion interpolation algorithm is beyond the scope of this paper. The integration of the VCRT maps with the engine performance simulation model are discussed in the following section.

2.3 Modelling of the VCRT in a turbofan Engine

The objective engine used in this paper is a twin-spool low bypass turbofan engine which employs the 1+1/2 type VCRT. A sketch of the objective engine, with station numbers, is shown in Figure 6. The definition of the station numbers are given in Table 1.

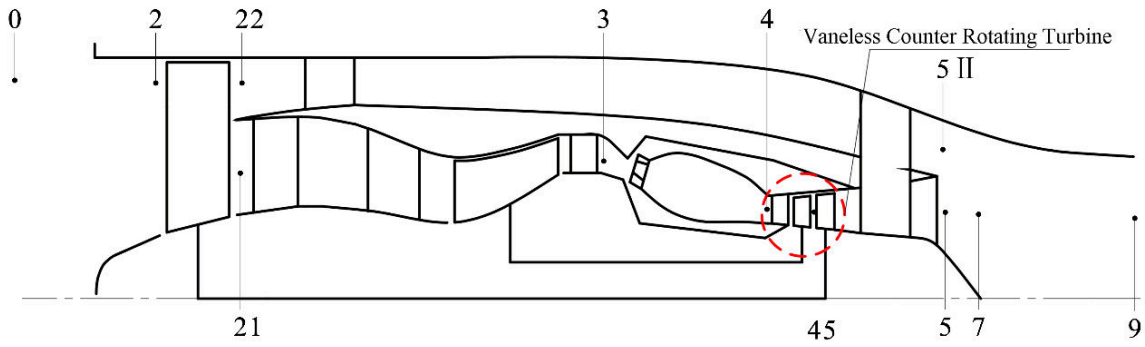

Figure 6. Sketch of two-spool mixed turbofan engine employing VCRT

Table 1
Engine station number definition

Station number	Definition
0	Ambient condition
2	Fan entrance
22	Fan exit / Bypass entrance
21	Fan exit / Compressor entrance
3	Compressor exit / Combustor entrance
4	Combustor exit / HP turbine entrance
45	HP turbine exit / LP turbine entrance
5	Turbine exit / Mixer entrance hot flow
5II	Bypass exit / Mixer entrance bypass flow
7	Mixer exit / Nozzle entrance
9	Nozzle exit

The performance simulation model of this VCRT turbofan engine is established by integrating VCRT maps with the component maps based simulation model. The steady state performance simulation model of a traditional twin-spool low bypass turbofan engine is presented in Table 2.[21, 22]

Table 2
Matching equations of twin-spool mixed turbofan engine

State factors	$\beta_{f,duct}$、$\beta_{f,core}$、β_c、T_4、N_l、$\pi_{t,h}$、$\pi_{t,l}$
Equations	$ERR_1=(m_{f,core} - m_c) / m_c$ $ERR_2=(m_{h,cor} - m'_{h,cor}) / m_{h,cor}$ $ERR_3=(m_{l,cor} - m'_{l,cor}) / m_{l,cor}$ $ERR_4=(L_{t,h} - L_c) / L_{t,h}$ $ERR_5=(L_{t,l} - L_f) / L_{t,l}$ $ERR_6=(P_{S5} - P_{S5II}) / P_{S5}$ $ERR_7=(P_7 - P_{7r}) / P_7$
Control parameter	N_h

Wherein, ERR_1-ERR_7 stand for error equations detected during the aero-thermodynamic calculation along the engine flow path. ERR_1 denote the mass flow balance equation between the core part fan and high pressure compressor. ERR_2, ERR_3 stand for the mass flow balance equation between combustor and HP turbine and that between HP turbine and LP turbine. ERR_4, ERR_5 denote the power balance between HP turbine and compressor and that between LP turbine and fan. ERR_6 stand for the mixer inflow static pressure balance. ERR_7 denote the nozzle mass flow balance.

As is shown in Table 2, 7 state factors are estimated and 7 error equations can be detected when performing the aero-thermodynamic calculation along the engine flow path. Consequently, a 7 dimensional nonlinear equation

group is established. The Newton-Raphson method is employed to iterate the state factors until all the equations are balanced and the matching point is found.

Since state factors and balance equations in the component maps based simulation model is partly determined by the turbine maps description and interpolation, they should be checked due to the implementation of the VCRT turbine maps. Four variables, $N_{h,cor}$, $\pi_{t,h}$, $N_{l,cor}$ and $\pi_{t,l}$, are needed to interpolate the corrected mass flow and the efficiency from those VCRT LP turbine maps. With N_h given as a control parameter, three other variables, N_l, $\pi_{t,h}$ and $\pi_{t,l}$, should be estimated as state factors. Additionally, two balance equations, i.e. the power balance between the LP turbine and the fan and the mass flow balance between the HP and LP turbine, can be detected. Compared with Table 2, the state factors and balance equations remain the same as in a conventional engine simulation model.

All in all, the difference between the VCRT engine model and the conventional one lies only in the fact that the former employs the quaternion interpolation method in the LP turbine map interpolation. This feature ensures minimum modification of the engine simulation model when using the new VCRT maps.

3.0 VALIDATION

A ground test of the relevant turbofan engine was performed on a ground test bed and the main steady state parameters were measured. This test data was corrected to the sea level international standard atmosphere (ISA) condition according to the similarity theory before it was used to validate the VCRT engine simulation model. More details of the experiment were introduced by Jia L.[22] Note that the values in Figure 7 are all relative values compared with design data.

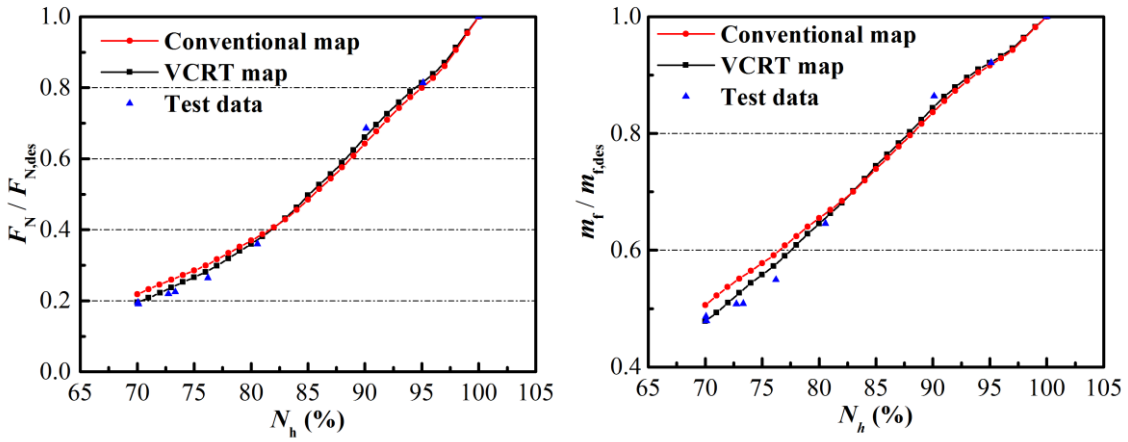

(a) Net thrust (b) Fan mass flow rate

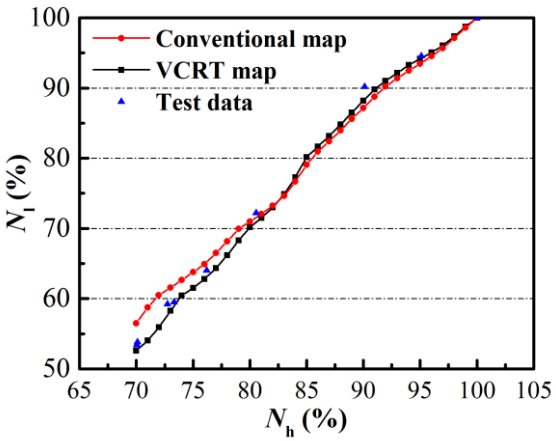

(c) Rotational speed of low pressure spool
Figure 7. Simulation results validation

Figure 7 shows the corrected test data and performance simulation results of the engine thrust F_N, the fan mass flow m_f, and the LP spool speed N_l, versus the HP spool speed N_h. The simulation results employing conventional turbine maps are also provided to show the difference between these two turbine map description methods. The data shown in these figures are all relative values.

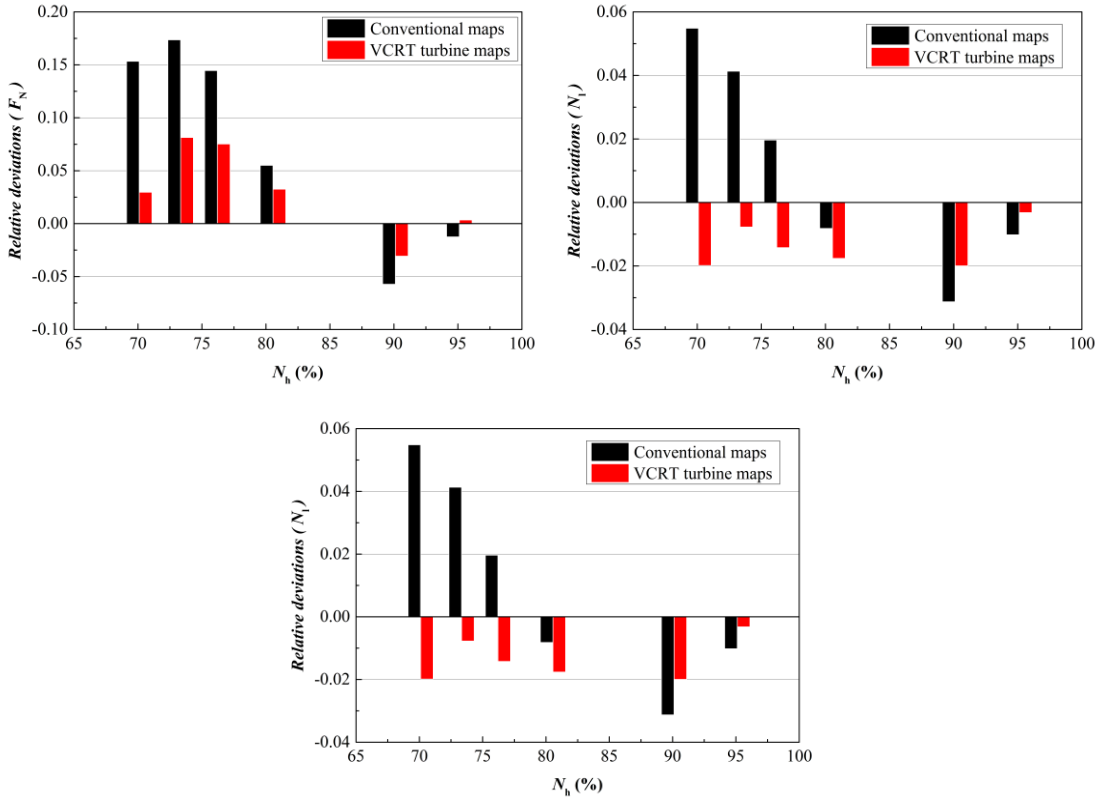

Figure 8. Deviations comparison of two methods

Figure 8 shows the relative deviations of the simulation results. As seen in Figure 8, in the region of $N_h > 80\%$, the deviations of both methods are within 5.5%. However, significant differences are detected under the condition of $N_h \leq 80\%$. The deviations of the new method is obviously smaller than those of the conventional method. The maximum relative deviations of F_N, m_f and N_l of the new method are 8.1%, 4.8% and 2.5% respectively, while these deviations for the conventional method are 17.4%, 9.3% and 6.0% respectively. These results indicate that the new method for counter rotating turbine modelling can improve the accuracy of engine performance simulation, especially for deep throttle conditions.

4.0 PERFORMANCE ANALYSIS

The new VCRT map description method ensures a higher fidelity VCRT engine performance simulation, making it reliable to analyse the influence of the VCRT on a gas turbine engine using simulation data. In other words, a comparison was performed between the performance simulation results of a VCRT engine and those of a conventional engine. The design parameters of these two engines are the same, except for their LP turbine assemblies. The VCRT engine uses the VCRT maps provided in the previous section. The conventional turbine maps used by the other engine is produced with the VCRT HP turbine rotational speed and pressure ratio fixed at design values.

4.1 Steady state performance simulation and analysis

The sea level ISA throttle performance of the two relevant engines were simulated. The simulation results are shown in Figure 9. Since the results of engine thrust, fan mass flow rate and LP rotational speed are already given in Figure 7, they will not be shown again here. Note that the values in Figure 9 are all relative values compared with design data.

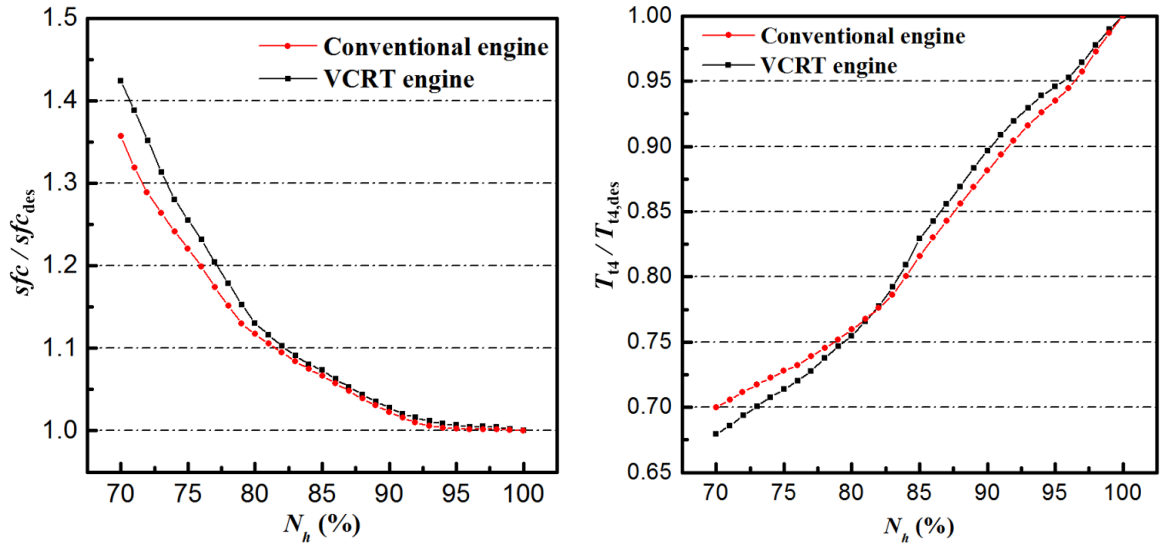

(a) Specific fuel consumption (b) Total temperature at NGV entrance

Figure 9. Throttle performance comparison

As seen in Figure 7 and Figure 9, in the region of $N_h \geq 80\%$ no significant difference in F_N, m_f and sfc is detected. However, when N_h is below 80%, F_N, m_f and T_4 of the VCRT engine are smaller, while the sfc becomes higher than those of the conventional one. These differences keep growing with the rotating speed decreasing. Take the state of $N_h = 70\%$ for instance, the F_N, m_f and T_4 of the VCRT engine are respectively 13%, 4% and 3% lower while the sfc is 4.5% higher.

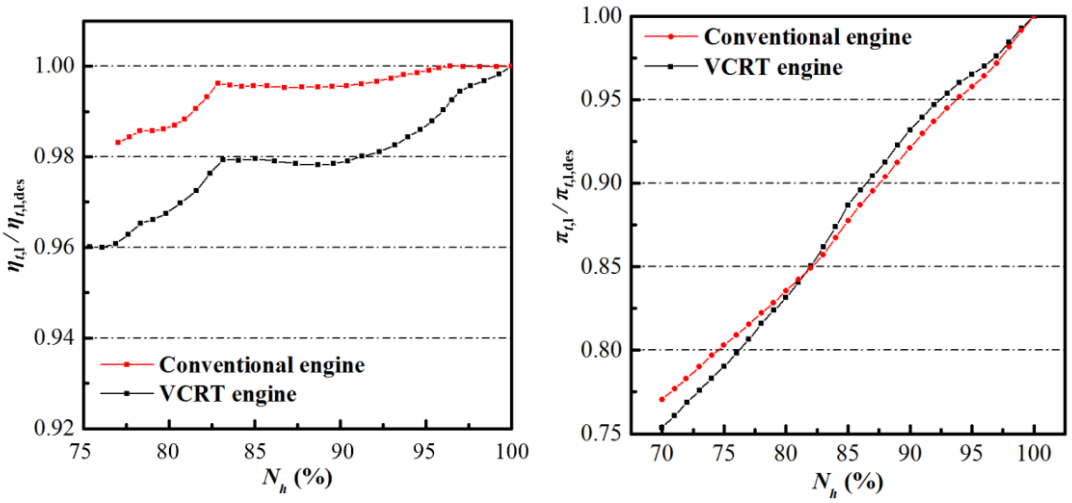

(a) Low pressure turbine efficiency (b) Low pressure turbine pressure ratio

Figure 10. Low pressure turbine performance in throttle rating

A conclusion can be drawn that the F_N, m_f and N_l of the VCRT engine all present a sharper decrease compared with those of the conventional engine during engine throttling. To fully understand how the VCRT influences the engine performance, the LP turbine performance is shown in Figure 10. Also, the specific work ratio ($SWR = l_{t,h} / l_{t,l}$) are provided in Figure 11.

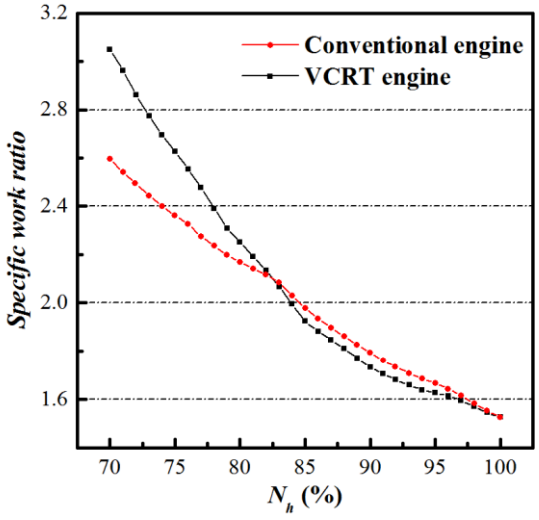

Figure 11. Specific work ratio vs. throttle setting

Again, the trend of $\pi_{t,l}$ is divided into two parts by the point of $N_h \approx 80\%$. On the right side, $\pi_{t,l}$ of the counter rotating turbine is larger than that of the conventional one, while the former is lower than the latter on the left side. Where $N_h = 70\%$, the $\pi_{t,l}$ of the counter rotating turbine is about 3% lower. However, along the throttle operating line, the $\eta_{t,l}$ of the counter rotating turbine is always lower. The difference reaches about 2% at the point of $N_h = 70\%$.

The efficiency trend is not contrary to the conclusions drawn by Ji L[3] and Louis[23] that the VCRT has the potential to maintain higher efficiency than a conventional turbine. Instead, it indicates the complicated mechanism and challenge of the VCRT on off-design points. To focus only on the off-design performance of the VCRT engine, the design turbine efficiency of these two engines were assumed to be the same. The lower efficiency detected in VCRT off-design operation is caused by the change of velocity triangles, as was discussed in the section of VCRT off-design features analysis.

A sharper decrease of the engine thrust is detected in the VCRT engine during engine throttling. The decrease of the engine thrust is attributed to both the decrease of the specific thrust and the engine mass flow. For the VCRT engine in the region of $N_h < 80\%$, on one hand, lower $\pi_{t,l}$ and $\eta_{t,l}$ result in lower LP turbine work and lower fan rotational speed, see Figure 11(a), which further causes a decrease of the fan mass flow, see Figure 9(b). On the other hand, the decrease of the fan rotational speed and the pressure ratio result in lower compressor mass flow. Further, the change of the velocity triangles causes both the HP turbine reaction degree and the SWR to increase, see Figure 11(b). In this circumstance, for a given N_h, the counter rotating engine works at lower T_4 and thus lower engine thrust.

The specific work of the VCRT LP turbine decreases more sharply than that of a conventional turbine during throttling. In other words, the SWR of a VCRT engine increases faster during this process. This trend provides evidence for Ji L's conclusion that the insufficient work capacity of the VCRT LP turbine under off-design conditions is a constraint to the application of the VCRT.[3] Flow control methods such as the suction surface bump in HP rotor, the variable HP guide vane, and the coolant injection in HP rotor are suggested and studied to obtain better off-design performance by the VCRT.[3, 13]

4.2 Transient performance simulation and analysis

The transient state performance of a gas turbine engine is a key to evaluate the engine availability. So the influence of a VCRT on engine transient performance, such as the transient duration and the operating line, is also investigated in this paper.

In engine transient maneuver, the change of thermodynamic parameters cause transient effects, such as the rotor acceleration and deceleration, the change of turbo machinery tip clearance, the storage of mass and energy in volumes and the heat suctions in engine structures. Refs. [24] and [25] offered some correlations to take these factors into consideration in an engine transient performance simulation model.

The transient effects are considered and the engine transient performance simulation model is developed based on the steady state simulation model. The engine transient performance simulation is in fact a matter of solving

differential equations. The implicit Euler scheme is utilized to establish the equations and again the Newton-Raphson method is used to solve them.

The transient performance of some counter rotating turbofan engine is simulated employing the transient performance simulation program. To indicate the effects of the VCRT on engine transient performance, the simulation results is again compared with that of a conventional turbofan engine.

4.2.1 Acceleration performance simulation and analysis

Given the same acceleration control schedule (Wfb/P_3 =f_5 (N_h)), engine acceleration performance is simulated. The acceleration interval is from 65% N_h to maximum N_h and the engine works at sea level ISA, Ma=0.0. (See Figure 12)

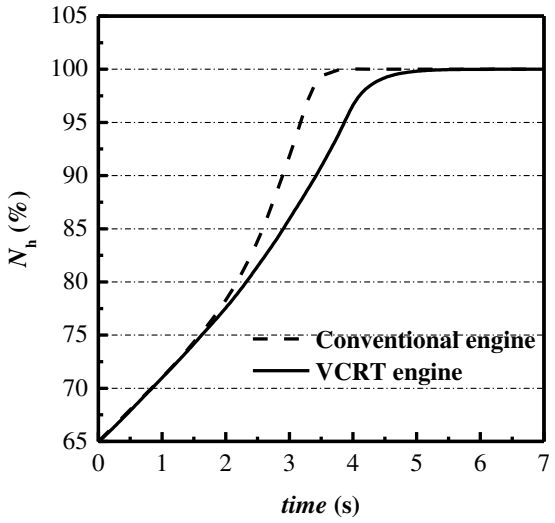

(a) HP spool rotating speed (N_h)

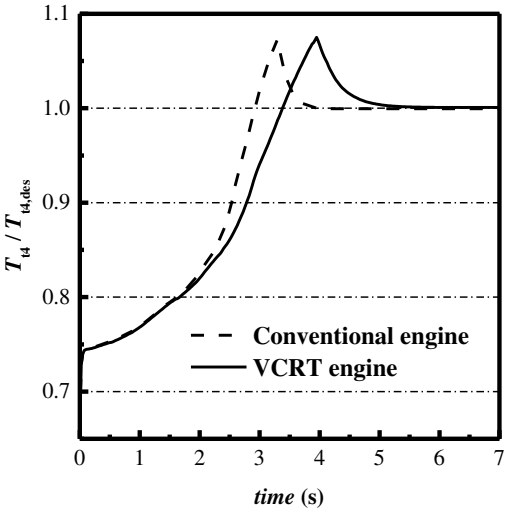

(b) Total temperature at turbine entrance (T_4)

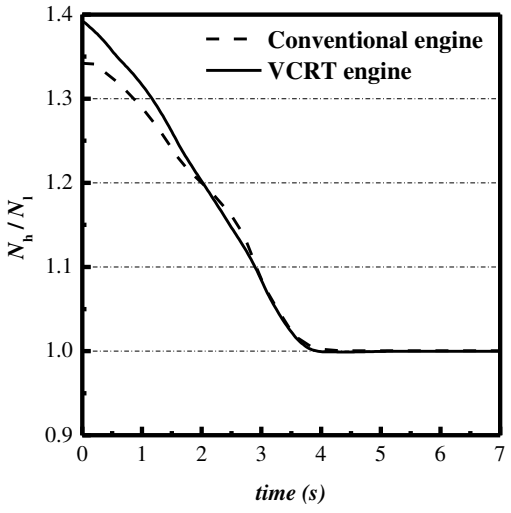

(c) Ratio of N_h to N_l

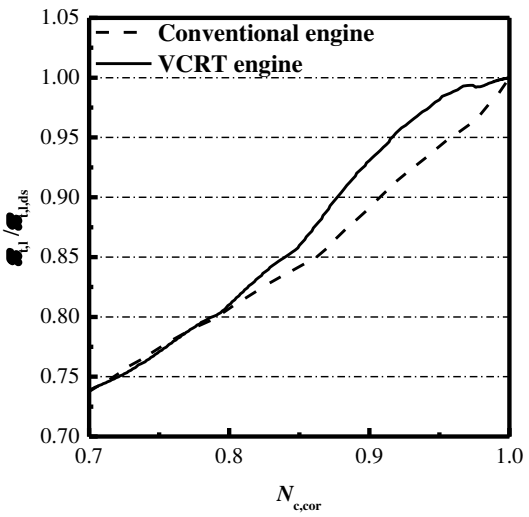

(d) Pressure ratio of LP turbine

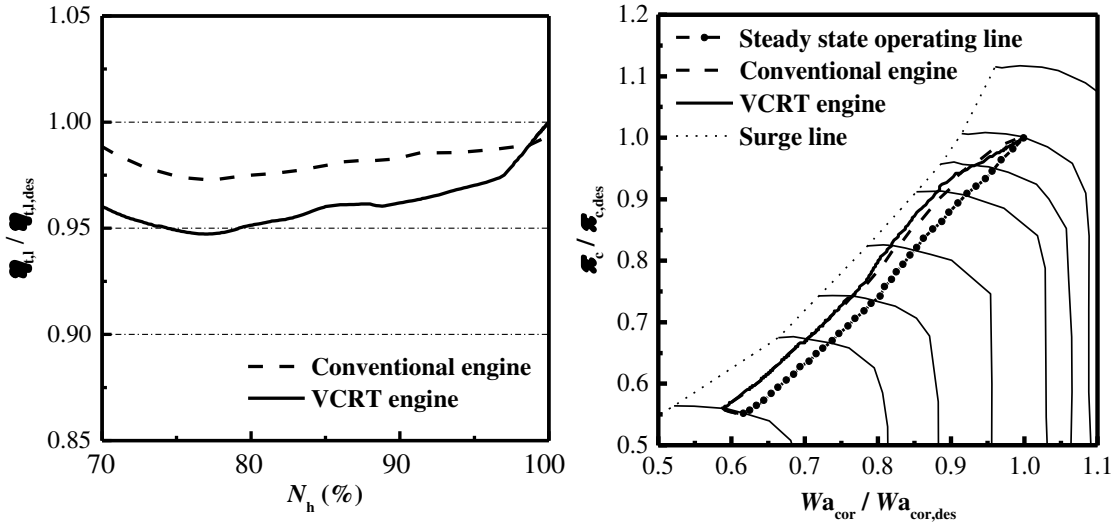

(e) LP turbine efficiency (f) Gas generator operating line

Figure 12. Counter rotating turbofan engine acceleration performance

As can be seen from Figure 12(a), given the same acceleration control schedule, the acceleration time of the VCRT engine is longer. The trend of the turbine inlet total temperature is similar and both encounter an over temperature of 5% of the designed T_4 (Figure 12(b)).

Figure 12(c) and Figure 12(e) illuminate the reason why a lag is detected in VCRT engine acceleration. For low N_h conditions, the changes of N_l and N_h cause the change of the velocity triangles of the LP turbine which finally leads to the decrease of both the LP turbine efficiency and the pressure ratio. Although the LP turbine efficiency and the pressure ratio of the VCRT engine is higher near design point, it can't make up the delays at the beginning of the acceleration.

In Figure 12(f), no significant difference is detected in the gas generator operating lines. This can also be explained using the gas turbine engine matching theory in which the operating line of the gas generator is regarded to be a single line with the LP turbine throat being critical or super critical.

4.2.2 Deceleration performance simulation and analysis

Given the same deceleration control schedule ($Wfb/P_3 = f_4(N_h)$), engine deceleration performance is simulated. The deceleration interval is from the maximum N_h to 65% N_h and the engine works at sea level ISA, Ma=0.0. (See Figure 13)

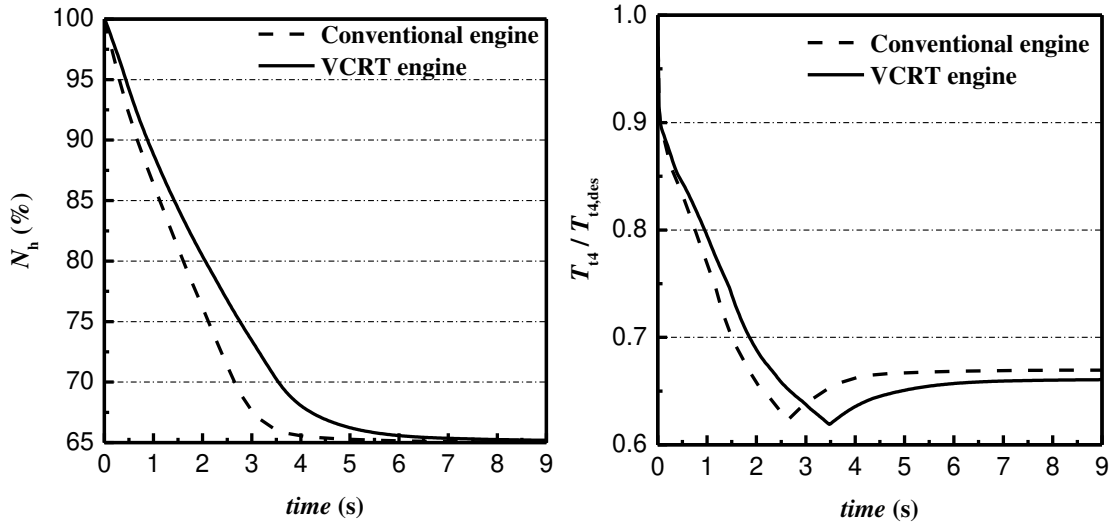

(a) HP spool rotating speed (N_h) (b) Total temperature at turbine entrance (T_4)

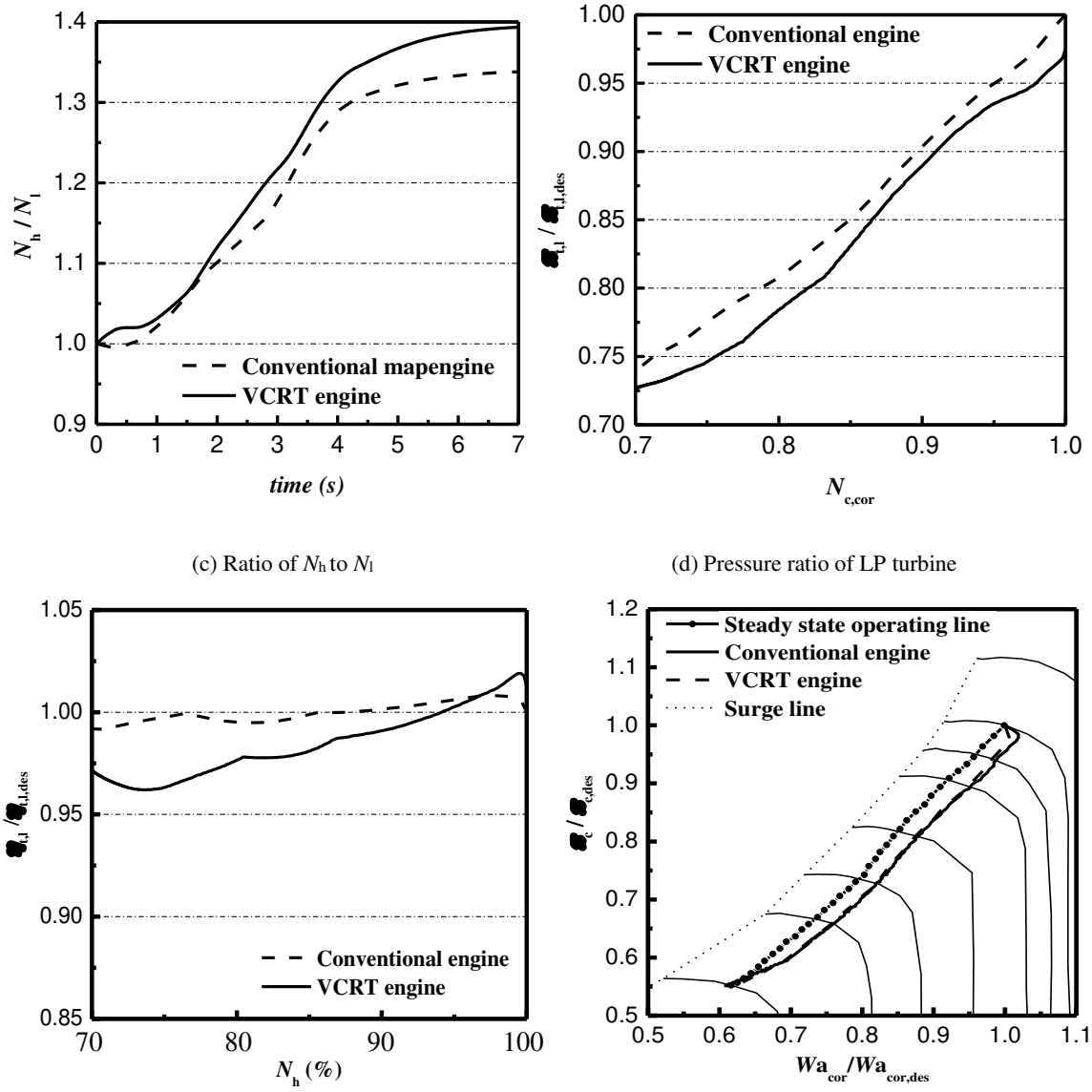

(c) Ratio of N_h to N_l (d) Pressure ratio of LP turbine

(e) LP turbine efficiency (f) Gas generator operating line

Figure 13. Counter rotating turbofan engine deceleration performance

As shown in Figure 13(a), the deceleration time of the counter rotating turbofan engine is longer than that of the conventional one, given the same deceleration control schedule. Also the trends of the turbine inlet total temperature are the same (Figure 13(b)).

The ratio of N_h to N_l for the counter rotating engine is higher (Figure 13(c)) because its fan rotating speed is lower at the same HP spool rotating speed. Meanwhile, the efficiency and the pressure ratio of the counter rotating LP turbine are also lower than those of the conventional one (Figures. 13(d) and 13(e)), which is conductive to engine deceleration. However, due to the reason that the ending LP rotating speed is lower, the deceleration time of counter rotating engine is still longer than that of the conventional one.

As is shown in Figure 13(f), no significant difference is detected in the gas generator operating lines during deceleration.

5.0 CONCLUSION

In this paper, a new method of the VCRT maps description was established. The maps are integrated with the engine performance simulation model and the simulation results of a low bypass turbofan engine were validated with test data. The influences of the VCRT on the engine performance was studied by means of comparing the performance of a VCRT engine with that of a conventional engine.

Validation results prove that, by considering the influence of the HP turbine on the LP turbine, the new method of the VCRT performance modelling can improve the accuracy of VCRT engine performance simulation.

In comparing the performance of these two engines, no significant difference is detected near design conditions. While under deep throttle conditions, the insufficient work capacity of the VCRT low pressure turbine is detected due to the decrease of both its efficiency and pressure ratio. Consequently, the engine thrust, the fan mass flow, the HP turbine inlet temperature and the LP spool rotating speed decrease while the specific fuel consumption increases. To improve the off-design performance of the VCRT engine, some flow control methods are suggested.

The VCRT maps description method and the VCRT turbofan engine simulation model introduced in this paper can be adjusted for other type of gas turbine engines which employ a VCRT. Also, the performance analysis can be a guide for VCRT engine design and analysis.

REFERENCES

[1] Gahn SM, Morris RW. Integrated high performance turbine engine technology. Online Referencing, http://www.pr.afrl.af.mil/divisions/prt (2006, accessed 14 October 2014).

[2] HEHS, ERIC. "F-22 Design Evolution, Part II," Code One Magazine, October 1998b." *As of April* 9 (2012).

[3] LUCHENG, J. "Analysis of technical challenges in vaneless counter-rotating turbomachinery." *ASME Paper No. GT2007-27617* (2007).

[4] MOROZ, LEONID, et al. "Comparison of counter–rotating and traditional axial aircraft low-pressure turbines integral and detailed performacnes." *Ichmt Digital Library Online*. Begel House Inc., 2009.

[5] FOLLEN, GREGORY, AND M. AUBUCHON. "Numerical zooming between a NPSS engine system simulation and a one-dimensional high compressor analysis code." (2000).

[6] RANSOM DL. Advancing jet engine design: An SwRI-led NPSS consortium helps design next-generation propulsion systems. *Technology Today*, Summer 2015.

[7] PACHIDIS, V., et al. "A de-coupled approach to component high-fidelity analysis using computational fluid dynamics." *Proceedings of the Institution of Mechanical Engineers, Part G: Journal of Aerospace Engineering* 221.1 (2007): 105-113.

[8] PACHIDIS, V., et al. "A comparison of component zooming simulation strategies using streamline curvature." *Proceedings of the Institution of Mechanical Engineers, Part G: Journal of Aerospace Engineering* 221.1 (2007): 1-15.

[9] SELLERS, JAMES F., and Carl J. Daniele. "DYNGEN: A program for calculating steady-state and transient performance of turbojet and turbofan engines." (1975).

[10] KURZKE, J. "GasTurb 12: A program to calculate design and off-design performance of gas turbines. User's manual." (2012).

[11] VISSER, WILHELMUS PETRUS JOSEF. "Generic Analysis Methods for Gas Turbine Engine Performance: The development of the gas turbine simulation program GSP." (2015).

[12] ZHAO, WEI, BING WU, and JIANZHONG XU. "Aerodynamic design and analysis of a multistage vaneless counter-rotating turbine." *Journal of Turbomachinery*137.6 (2015): 061008.

[13] Qiao J. "*Investigation on aerodynamic optimization design and hot streak effects in counter-rotating turbine.*", PhD Thesis, Graduate University of Chinese Academy of Sciences, Beijing, China, May 2012.

[14] QINGJUN, ZHAO, et al. "Influence of hot streak temperature ratio on low pressure stage of a vaneless counter-rotating turbine." *Journal of Engineering for Gas Turbines and Power* 130.3 (2008): 031901.

[15] QINGJUN, ZHAO, et al. "Tip clearance effects on inlet hot streak migration characteristics in high pressure stage of a vaneless counter-rotating turbine." *Journal of Turbomachinery* 132.1 (2010): 011005.

[16] LUO W. "*Investigation of performance based on flow control in a vaneless counter-rotating turbine.* ", PhD Thesis, Graduate University of Chinese Academy of Sciences, Beijing, China, May, 2012.

[17] Wang W. "Investigation of flow and film cooling performance of new cooling hole geometry and film cooling of gas turbine." PhD Thesis, Graduate University of Chinese Academy of Sciences, Beijing, China, May, 2012.

[18] HUBER, F., et al. "Design and test of a small two stage counter-rotating turbine for rocket engine application." *29th Joint Propulsion Conference and Exhibit*. 1993.

[19] LIU, SI-YONG, et al. "Research on aerodynamic design of counter-rotating turbine without intermediate vanes [J]." *Gas Turbine Experiment and Research* 1 (2002): 006.

[20] SUBBARAO, RAYAPATI, AND M. GOVARDHAN. "Effect of speed ratio on the performance and flow field of a counter rotating turbine." *Energy Procedia* 54 (2014): 580-592.

[21] CHEN, YU-CHUN, et al. "Virtual power extraction method of designing acceleration and deceleration control law of turbofan." *45th AIAA/ASME/SAE/ASEE Joint Propulsion Conference & Exhibit*. 2009.

[22] JIA L, CHEN Y, HUANG X, et al. "Effect of 1+1/2 counter rotating turbine on twin-shaft mixed turbofan engine.", *Propulsion Technology* 2013; 34(11): 1459-1465.

[23] J. F. LOUIS, "Axial flow contra-rotating turbines." *ASME paper* 85-GT (1985): 218.

[24] P. P. WALSH, P. FLETCHER, "Gas Turbine Performance." Chapter 8, Transient Performance, Second Edition, Oxford: Blackwell Science Ltd, 2004, 444-465.

[25] C. RIEGLER, "Correlations to include heat transfer in gas turbine performance calculations.", *Aerospace Science and Technology*, 1999, 3(5) 281-292,

Modelling and performance analysis of vaneless counter rotating turbine in gas turbine engines

Jia, Linyuan

2017-09-08

Jia L, Chen Y, Gao Y, Zhao J. (2017) Modelling and performance analysis of vaneless counter rotating turbine in gas turbine engines. In: ISABE 2017: 23rd International Symposium on Air Breathing Engines: Economy, Efficiency and Environment, 3-8 September 2017, Manchester, UK. Paper number ISABE-2017-21476

https://www.isabe.org/